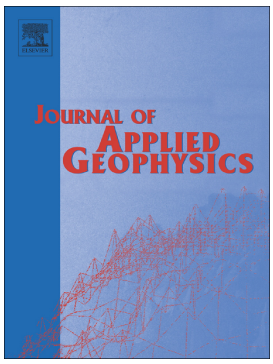

How close can we get to the classical magnetotelluric sounding?

Armando Calderón-Moctezuma, E. Gomez-Treviño, V. Yutsis, R. Guevara-Betancourt, Marianggy Gómez-Ávila

PII: S0926-9851(22)00136-7

DOI: https://doi.org/10.1016/j.jappgeo.2022.104665

Reference: APPGEO 104665

To appear in: *Journal of Applied Geophysics*

Received date: 20 March 2021

Revised date: 27 April 2022

Accepted date: 2 May 2022

Please cite this article as: A. Calderón-Moctezuma, E. Gomez-Treviño, V. Yutsis, et al., How close can we get to the classical magnetotelluric sounding?, *Journal of Applied Geophysics* (2021), https://doi.org/10.1016/j.jappgeo.2022.104665

How close can we get to the classical magnetotelluric sounding?

Authors: Armando Calderón-Moctezuma[1,2], E. Gomez-Treviño[3], V. Yutsis[1], R. Guevara-Betancourt [1,4] and Marianggy Gómez-Ávila [5].

[1]División de Geociencias Aplicadas, Instituto Potosino de Investigación Científica y Tecnología A.C.; Camino a la Presa San José 2055, Lomas 4ta Sección, C.P. 78216, San Luis Potosí, San Luis Potosí, México.

[2]Instituto de Investigaciones en Matemáticas Aplicadas y en Sistemas, Universidad Nacional Autónoma de México; Circuito Escolar 3000, Ciudad Universitaria, C.P. 04510, Coyoacán, México City, México

[3]División de Ciencias de la Tierra, Centro de Investigación Científica y de Educación Superior de Ensenada; Carretera Ensenada-Tijuana 3918, Zona Playitas, C.P. 22860, Ensenada, Baja California, México.

[4]Instituto de Geología, Universidad Autónoma de San Luis Potosí; Av. Dr, Manuel Nava 330A, San Luis Potosí, San Luis Potosí, México.

[5]Instituto de Ingeniería y Tecnología, Universidad Autónoma de Ciudad Juárez, Ciudad Juárez, Chihuahua, 32310, México.

Corresponding author: a.calderonmoctezuma@gmail.com

Abstract

The classical magnetotelluric (MT) sounding can be defined as data that are invariant under rotation of coordinates -a feature we call centrality- and are affected solely by electromagnetic induction effects –a feature we call all-induction. The classical sounding can be realized only in the case of laterally isotropic media and perfectly horizontal layering. However, in general it is possible to process data from several sites to make an approximation. For instance, the electromagnetic array profiling (EMAP) method addresses the issue of all-induction by means of spatial filtering. The method is very effective but its application is not practical for long profiles because it requires too many contiguous dipoles. A more practical version exists that does not require contiguous dipoles but neither of them addresses the centrality issue; in the first case because the data are taken along a single direction, and in the other because it uses traditional orthogonal modes. In this work we improve over the last approach by introducing centrality to make the approximation closer to the classical sounding. We use the determinant of the impedance tensor, which is the only invariant among all that are known that can handle centrality, the galvanic distortions and also the isolation of all-induction effects through two-dimensional inversion. This approach to the classical MT sounding is illustrated using the synthetic dataset COPROD2S2 and the field dataset BC87 from British Columbia, Canada, which are commonly used for testing new ideas. We also apply it to a recent profile over the Colima Graben, México.

Keywords: Magnetotelluric; all-induction; determinant; COPROD2S2; BC87; classical MT sounding.

1. Introduction

Tikhonov (1950), Rikitake (1950) and Cagniard (1953) all conceived the magnetotelluric (MT) method assuming isotropic and perfectly horizontal layered media. This is what we now call a one-dimensional (1D) model. Although this model seldom applies in practice it provides two features that are worth trying to reproduce with field data. One is that the response of the subsurface resistivity distribution is invariant under rotation of coordinates, a feature we call centrality. In general, central or invariant soundings have special appeal because of their natural uniform averaging character around the point of measurement. This is one of the reasons for the popularity of controlled-source central soundings, particularly in their time-domain version. They are interpreted assuming a 1D model and then used to calibrate the depth of penetration of MT soundings (e.g., Stemberg et al., 1988).

Besides invariance under rotation, the other attractive feature of controlled-source central soundings is that they are an approximation to a purely electromagnetic induction response regardless of dimensionality. This is the other feature of the classical MT sounding: that of responding solely to electromagnetic induction effects. In both cases we can refer to them as all-induction soundings, in the sense that electric charges have very little or no effects on the overall response. In this work we present an approximation to the classical MT sounding by addressing together the two features mentioned above: invariance under rotation and isolation of electromagnetic induction effects.

There may be several ways to approximate to the classical MT sounding. For one thing, there are plenty of invariants of the impedance tensor to choose from to meet the first requirement (e.g., Szarka and Menvielle, 1997). One thing to consider is how particular invariants are compatible with the second requirement of isolating electromagnetic induction. The other thing to consider is that, in principle, it is not possible to separate for a given response the part that comes from electromagnetic induction from that that comes from electric charges that accumulate at surfaces of discontinuity. It is possible only for small, near surface anomalies. This is what we do when correcting for statics using controlled-source central soundings, or when applying the Groom-Bailey (1989) approach to deal with the other two galvanic distortions. In general, the effects of electric charges from deeper regions are always present unless something deliberate is done about them.

The first approximation to the classical MT sounding is described by Bostick (1984) in his patent of the Electromagnetic Array Profiling or EMAP method. Of the two features mentioned above: 1) rotational invariance and 2) all-induction, EMAP centers on the latter. This is achieved by means of contiguous dipoles along a profile to measure electric fields. There is always a common electrode for two contiguous dipoles, except for those at both ends of the profile. All-induction is achieved by averaging with special filters a number of measurements in such a way that the galvanic effects tend to cancel at the common grounding points. Using an electrode twice, positive for one dipole and negative for the next, the galvanic effects cancel. This is done in a scale-free fashion by using the skin depth as the measure of length, both vertically and horizontally along the profile. The result is

the rejection of galvanic effects at all depths, not only those associated with small, near-surface anomalies. In the EMAP approach if the skin depth is very large the so called small, near surface anomalies increase both in size and depth. The result is all-induction soundings by removing the effect of electric charges from all depths. The corresponding apparent resistivities are then inverted using the one-dimensional (1D) Bostick (1977) transformation to obtain two-dimensional (2D) images. Although the EMAP method is very effective it is not widely used because it requires too many contiguous dipoles for a typical survey. This explains why there are relatively few papers on the subject. The reader is referred to the patent of Bostick (1984) and to the papers by Bostick (1986) and Robertson (1989), the PhD thesis of Torres-Verdín (1991), and the papers by Torres-Verdín and Bostick (1992a, 1992b) and Esparza and Gómez-Treviño (1997). As stated earlier, the EMAP method addresses the issue of all-induction at the cost of many contiguous electric dipoles.

It is possible to address the issue of all-induction by using non-contiguous electric dipoles. Gómez-Treviño et al. (2014) use the transverse electric (TE) mode as a natural filter for the effect of electric charges from all depths. The role of the contiguous dipoles in EMAP is approximated by a series of steps. First, the apparent resistivities of the TE mode are left out of a 2D inversion because they cannot be reproduced by a 2D model when static effects are present. The rest of the data is fitted as much as possible in detriment of the smoothness of the model, contrary to the Occam philosophy (Constable et al., 1987). The results are very rough models that are difficult to make sense of because of the very large spatial frequencies. The degree of roughness is stopped when the computed TE apparent

resistivities for the models converge to a stable value. The corresponding TE apparent resistivities, which are free from the effect of electric charges from all depths, are then inverted using a 1D formula for depth averages of electrical conductivity to obtain 2D images. As in the case of EMAP this method also centers on the all-induction feature of the classical MT sounding.

Neither of the two approximations described above addresses the rotational invariant character of the ideal MT sounding. Obviously, the way to proceed forward is to use invariants of the impedance tensor. They have been used in the past to deal with a variety of practical issues through 2D inversions (e.g. Pedersen and Engels, 2005; Romo et al., 2005; and Wang et al., 2020). However, the all-induction part of the ideal sounding has never been considered together with invariants to approximate the ideal sounding. In this respect, the issue to be resolved is which of the known invariants lends itself to blend together with the all-induction part.

It has been a while since the development of three-dimensional (3D) algorithms (e.g., Mackie et al., 1993; Siripunvaraporn et al., 2005). At present, the state of the art is such that most MT surveys are interpreted using 3D tools (e.g. Wang et al., 2019; Shi et al., 2020; Ruiz-Aguilar et al., 2020). Why then go back in time to 1D models? One of the reasons we should explore the past is that 1D models were actually never realized in practice. In other words, they were never proved to be inferior to 2 o 3D models. They were just jumped over because it was soon discovered that MT measurements could only be characterized by a tensor, and not by a scalar. In addition, considering 1D models is not necessarily a step back in time because back then we didn't understand 3D galvanic distortions, and

much less how to remove them. We neither understood the effects of electric charges from all depths nor how to remove them. The issue is that now we can enquire with some propriety how close can we get to the ideal sounding. Beyond academic curiosity there are practical issues. Consider for instance one of the original assets of the MT method, that of detecting good conductors without the somewhat annoying interference of good resistors.

2. The unique place of the determinant

In this section we claim that the determinant of the impedance tensor is the only invariant that can handle all galvanic distortions in accord with the further requirement of separating electromagnetic induction effects from those of electric charges at all depths.

The natural electric fields that are of interest in the MT method may be distorted by small, near surface anomalies that are of no significance for deep explorations (e.g., Bahr, 1988; Jiracek, 1990; Zhdanov and Keller, 1994). However small, these anomalies can alter the electric fields by orders of magnitude, so they have to be dealt with, for otherwise they may lead to doubtful images of the subsurface (Berdichevsky et al., 1998). The first thing to do to acknowledge their existence is to express their effect mathematically. Assuming linearity the measured components $\mathrm{E_{mx}}$ and $\mathrm{E_{my}}$ are related to the undistorted components $\mathrm{E_x}$ and $\mathrm{E_y}$ through the equation

$$\begin{pmatrix} E_{mx} \\ E_{my} \end{pmatrix} = \begin{pmatrix} C_{11} & C_{12} \\ C_{21} & C_{22} \end{pmatrix} \begin{pmatrix} E_x \\ E_y \end{pmatrix}. \qquad (1)$$

The constants C_{ij} are real and do not depend on frequency. The equation applies to anomalies smaller and closer to the electric line than a skin depth. This means that electromagnetic induction effects are negligible as compared with galvanic or direct-current (DC) effects. This is why they affect only the magnitude of the electric field and not the phase. They are independent of frequency because the DC effects are also independent of frequency. In 2D when the axes are orthogonal to the profile $C_{12} = C_{21} = 0$. In this case C_{11} acts as a static factor that shifts the corresponding apparent resistivities upwards or downwards in a log scale, and C_{22} shifts the other mode accordingly. In general, the constants C_{12} and C_{21} account for three-dimensional (3D) distorting anomalies by acknowledging that a given component can be affected by currents in orthogonal directions.

Once expressed mathematically, the distortion concept entered into main stream research (e.g., Bahr, 1988; Groom and Bailey, 1989). Translating equation (1) into impedance language it can be written that the undistorted impedance is equally affected by the distortion matrix. Explicitly

$$\begin{pmatrix} Z_{mxx} & Z_{mxy} \\ Z_{myx} & Z_{myy} \end{pmatrix} = \begin{pmatrix} C_{11} & C_{12} \\ C_{21} & C_{22} \end{pmatrix} \begin{pmatrix} Z_{xx} & Z_{xy} \\ Z_{yx} & Z_{yy} \end{pmatrix}. \qquad (2)$$

In compact form this can be written as

$$\mathbf{Z}_m = \mathbf{CZ} \ . \qquad (3)$$

Rotating $\mathbf{Z}_{\mathrm{m}}$ through a rotation matrix $\mathbf{R}$ the result can be written for an arbitrary coordinate system as

$$\mathbf{Z}_{\mathrm{mR}} = \mathbf{RCZR}^{\mathrm{T}} \ . \qquad (4)$$

Take the determinant on both sides of this equation. Considering that $\mathrm{Det}(\mathbf{R}) = \mathrm{Det}(\mathbf{R}^{\mathrm{T}}) = 1$ the result is

$$\mathrm{Det}(\mathbf{Z}_{\mathrm{mR}}) = \mathrm{Det}\,(\mathbf{C})\mathrm{Det}(\mathbf{Z}) \ . \qquad (5)$$

This means that the rotated and the original impedances have the same determinant. In other words, that their determinant is invariant under rotation. We now turn to how the distortion matrix $\mathbf{C}$ has been factorized in the literature. In particular, to what is known as the tensor decomposition of Groom and Bailey (1989). The factorization is given as

$$\mathbf{C} = \mathbf{TSA} \ . \qquad (6)$$

The explicit form of each matrix is given in Table 1. What is our interest here is the determinant of the distortion matrix $\mathbf{C}$ to substitute it in equation (5). Using the expressions given in Table 1, it follows that

$$\mathrm{Det}(\mathbf{T}) = 1 \ , \qquad (7)$$

$$\mathrm{Det}(\mathbf{S}) = \frac{1 - \mathrm{e}^2}{1 + \mathrm{e}^2} \qquad (8)$$

and $$\mathrm{Det}(\mathbf{A}) = \mathrm{ab} \ . \qquad (9)$$

Substituting these expressions in equation (5) it follows that

$$\mathrm{Det}(\mathbf{Z}_{\mathrm{m}}) = \mathrm{ab}\,\frac{1-\mathrm{e}^2}{1+\mathrm{e}^2}\,\mathrm{Det}(\mathbf{Z}\quad). \qquad (10)$$

The determinant of the distorted tensor is simply a scaled version of the determinant of the undistorted 2D impedances. This means that the determinant reduces the distortion matrix $\mathbf{C}$ to a single factor. There are still three unknowns: the two scaling factors $\mathrm{a\ and\ b}$ and the shear parameter e. However, the fact that they appear as a single factor separates apart the determinant from all other known invariants, as discussed below. The point is that this composed factor, which is real and independent of frequency, plays the role of a single static factor which can potentially be modeled by the TM mode.

All 2D modeling approaches solve for the TE and TM modes independently from each other (e.g., Wang et al., 2020). The determinant is then computed as the product of the two impedances. Thus, fitting a scaled or distorted determinant will require for the TM mode to accommodate the composed factor, not only its own static factor. The electric charges near the surface would be different in each case, but the end result would still be a constant for all periods. The particular value of the constant is not important as long as it is recovered as a constant and that the determinant data is fitted properly. The same applies to modeling in 2D the static effects of what in general are 3D small surface anomalies. As shown in the following sections, static factors for both TE and TM curves can be obtained from the determinant data.

Groom-Bailey decomposition for the determinant	
$\boldsymbol{Z_m = RTSAZ_2R^T}$	
Rotation	Twist
$\boldsymbol{R} = \begin{pmatrix} cos\theta & sin\theta \\ -sin\theta & cos\theta \end{pmatrix}$	$T = \frac{1}{\sqrt{1+t^2}}\begin{pmatrix} 1 & -t \\ t & 1 \end{pmatrix}$
$S = \frac{1}{\sqrt{1+e^2}}\begin{pmatrix} 1 & e \\ e & 1 \end{pmatrix}$	$A = \begin{pmatrix} a & 0 \\ 0 & b \end{pmatrix}$
Shear	Scaling
$Det(\boldsymbol{Z}_m) = ab\ \frac{1-e^2}{1+e^2}\ Det(\boldsymbol{Z}_2)$	

Table 1. The Groom and Bailey (1989) decomposition of the magnetotelluric impedance tensor. The tensor $\boldsymbol{Z}_2$ represents the undistorted impedances and it is assumed to be 2D. The tensors $\boldsymbol{T}$ and $\boldsymbol{S}$ introduce the 3D character of the distortions. Notice that the determinant of the distorted tensor is simply a scaled version of the determinant of the undistorted 2D impedances.

As a final point, it is important to remark that the determinant is the only invariant that without further processing can absorb all distortions through a multiplicative constant. This happens for the full 3D problem as indicated by equation (5). The explicit form given by equation (10) corresponds to what is called

the 3D/2D case using the Groom-Bailey factorization. Consider the invariant given by the sum of squares of the elements of the impedance tensor (Szarka and Menvielle, 1997). This is

$$ssq_m = Z_{mxx}^2 + Z_{mxy}^2 + Z_{myx}^2 + Z_{myy}^2 . \quad (11)$$

In 2D ssq_m is immune to twist and shear but not to the scaling factors $a \text{ and } b$ as demonstrated in Gómez-Treviñoet al., (2013). This means that in 2D

$$ssq_m = a^2 z_{xy}^2 + b^2 z_{yx}^2 . \quad (12)$$

Unless *a=b=1* we will have in general that $ssq_m \neq ssq$. The static factors modify separately the two undistorted impedances. In the case of the determinant the factors appear as products multiplying the undistorted determinant. In 2D equation 10 can be written as $Det(\boldsymbol{Z}_m) = kZ_{xy}Z_{yx}$ where *k* is an arbitrary constant that can be absorbed as a static effect by the apparent resistivities of the TM mode. The determinant, first introduced by Berdichevsky and Dmitriev (1976), is the only invariant of the seven independent invariants determined by Szarka and Menvielle (1997) that combines the scaling factors as a single product with the impedances. All others involve addition operations that mix the statics of the two modes as in equation 12. Along with the determinant the ssq has other interesting properties (e.g., Rung-Arunwan et al., 2016; 2017) but for the present problem the former is the most adequate.

3. Isolation of electromagnetic induction

Once the issue of which invariant is the most appropriate, we now turn to the all-induction part. This involves 2D inversion of the determinant data. The final result is obtained in two steps. We first overfit the data to obtain the roughest model in contrast to the traditional smoothing philosophy. The roughing process stops when the computed apparent resistivities of the TE mode converge. These resistivities, which are free from the effects of electric charges from all depths, are interpreted in 1D to obtain a 2D image of the subsurface below the profile. The procedure is summarized in the flowchart shown in Figure 1.

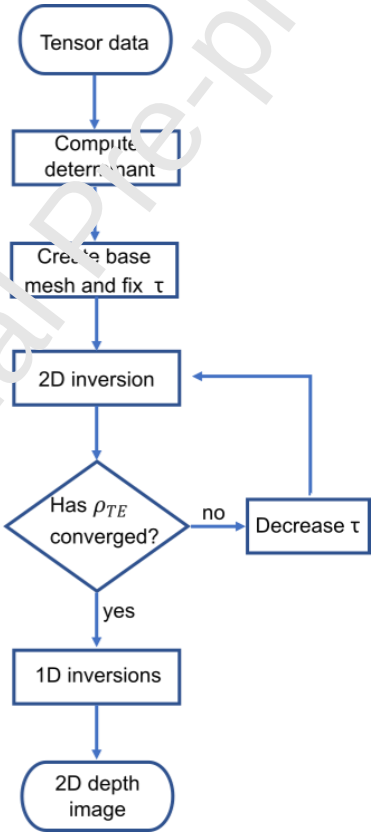

Figure 1. Flowchart that summarizes the procedure to go from the tensor data to the classical, rotationally invariant and all-induction magnetotelluric sounding. The 2D depth image is obtained assuming that at each site along a profile the data corresponds to a vertical sounding interpretable in 1D.

We tested our approach using a synthetic dataset that was proposed by Varentsov (1998, 2002) to compare different inversion methods. The theoretical TE and TM responses were contaminated with 5% random noise, static effects, some outliers and possibly a global displacement of all the apparent resistivity curves. The dataset is known as COPROD2S2 and is available at the MTNet site. There are 33 sites along a 50 km profile and 8 periods per site, from 1 to 3,000 s. The original sections are shown in Figure 2.

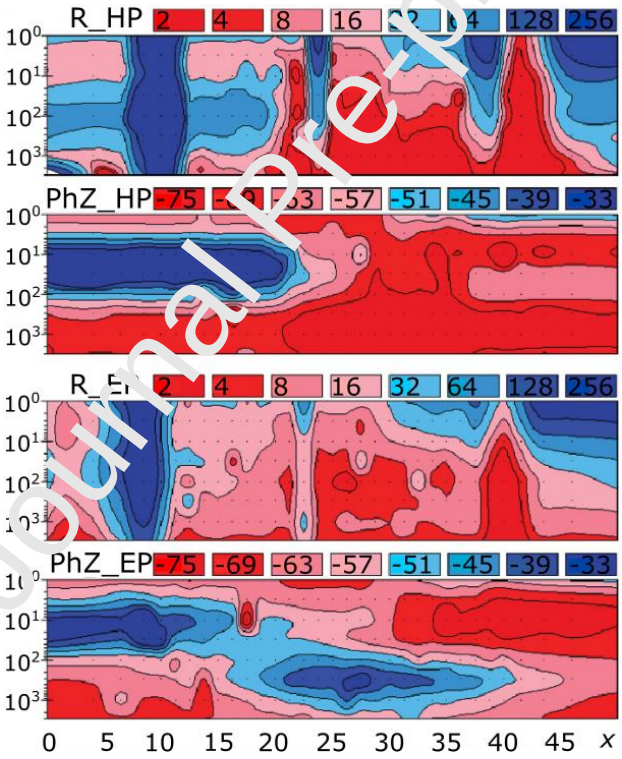

Figure 2. Original COPROD2S2 data. The original COPROD2S2 data as presented by Varentsov (1998). From top to bottom: TM mode apparent resistivity (R_HP) and impedance phase (PhZ_HP), TE mode resistivity (R_EP) and impedance phase (PhZ_EP). For all the sections, the vertical axis are periods in seconds and the horizontal is the distance in km. The apparent resistivity is in Ohm.m and the phase in degrees.

The dataset has been used by Ogawa (1999), Toumerie et al., (2007) and Gómez-Treviño et al., (2014) to test different methods for dealing with static effects. The results compare reasonably well between each other, although no comparison is made with the true model and the assumed static factors because they have not been released. The criteria for a good performance can only be judged by comparison with published results.

The pseudo-sections of the determinant are shown in Figure 3. The apparent resistivities were computed as the geometric average of the TE and TM resistivities, and the phases as the arithmetic average of the corresponding phases. Notice that the static shifts in the determinant are closely related to the shifts of the original TE and TM shown in Figure 2. In both cases the static effects appear as sharp vertical bands of color that affect the image from top to bottom. They would disappear for the determinant only when the factor of one mode is the reciprocal of the other, something that is very unlikely. On the other hand, the outliers appear as local color changes with very limited vertical extent. They are better appreciated in the phases.

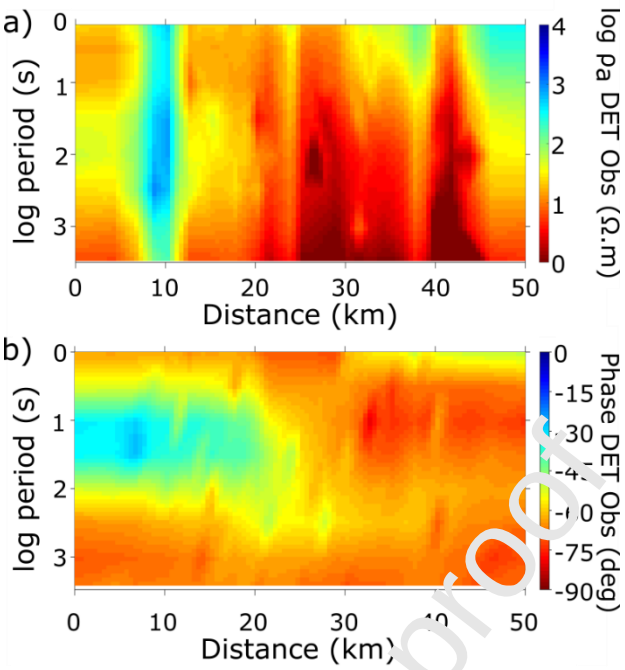

Figure 3. Determinant of COPROD2S2 data. a) Magnitude of the determinant apparent resistivity in logarithmic obtained as the geometric average of the corresponding TE and TM resistivities shown in Figure 1. b) The phase of the determinant impedance in degrees obtained as the arithmetic average of the corresponding TE and TM phases shown in Figure 2.

Consider the operation of going from Figure 2 to Figure 3 as a forward problem. It is definitely a stable process with a unique solution. Now consider the operation of going from Figure 3 to Figure 2. At first sight this would be impossible because the number of unknowns is twice the number of constraints. Simply put, one cannot recover two numbers when all you know is their average. Fortunately, Figures 2 and 3 share a common physical model of which both are responses on the surface of the ground. If we can find this model using the determinant of Figure 3 it is then a matter of computing its TE apparent resistivities and we reach the objective. These resistivities are all-induction responses that were derived from an

invariant that requires no identification of modes. This contrasts with the approach described by Gómez-Treviño et al. (2014) that uses the original TE and TM responses to obtain all-induction responses. It also contrasts with a later version of using invariant TE ant TM because this still requires identifying modes to make the inversion (Muñiz et al., 2017; Gomez-Treviño et al., 2018; Montiel-Alvarez et al., 2020). To fit the data, we use the 2D algorithm of Rodi and Makie (2001) modified to handle apparent resistivities and phases obtained from the determinant. To explain how we use the algorithm consider the penalty function

$$\mathrm{P} = \{\text{misfit of data} + \tau(\text{smoothness of model})\} \ .$$

The regularizing parameter τ is usually selected in such a way that there is a balance between the fit to the data and the smoothness of the model (e.g. Constable et al., 1987). The objective is to fit the data reasonably well and at the same time keep away from features not required for that fit. The way we use the algorithm handles this issue in a different way. What we do is to find the smallest possible value of τ that makes the output converge. The output in our case is not the model but the TE apparent resistivities of the model. We monitor the geometric average over period of the computed TE apparent resistivities for each site. The convergence test is shown in Figure 4. It can be observed that the curves converge for $\tau < 0.1$ and that for $\tau = 0.01$ and $\tau = 0.001$ the averages are practically identical.

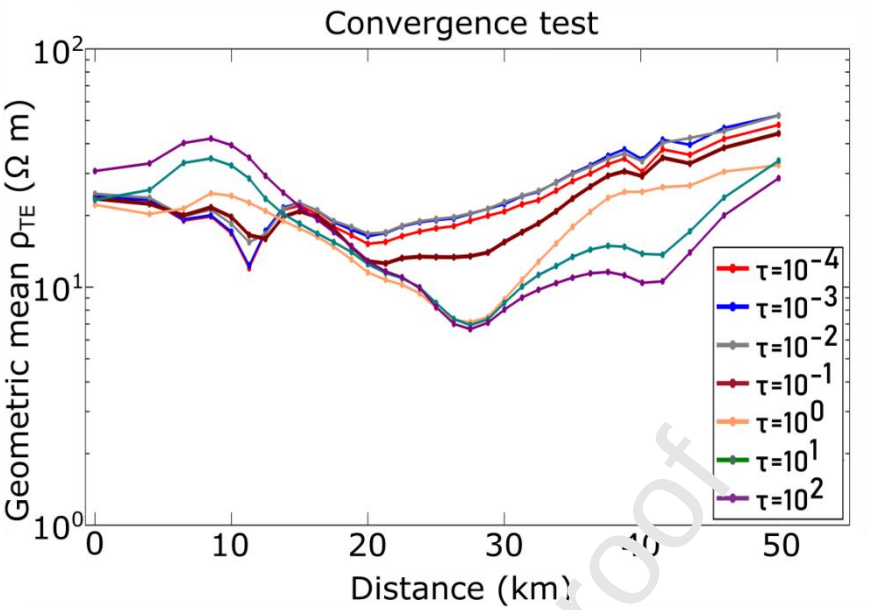

Figure 4. Convergence COPROD2S2. Convergence of the geometric mean of the computed apparent resistivities for the 33 sites. The y-axis represents the geometric mean of the TE apparent resistivity. Notice that the curves for $\tau = 0.01$ and $\tau = 0.001$ are practically identical. The curves converge for < 0.1.

Figure 5 shows the model corresponding to $\tau = 0.01$. We call this the base model. The first thing to notice is the relatively large lateral variations of resistivity at shallow depths. This is a desired property of the model because it allows an excellent fit to the data as can be appreciated in Figures 6a and 6b for apparent resistivities and in Figure 6c and 6d for the phases. In Figures 6a and 6c, the vertical strips due to static effects are very well reproduced. It can also be observed that the outliers are not reproduced by the computed apparent resistivities, they are all ignored in view of the rest of the data, even though they were not given larger errors, and despite of the smallness of the regularizing factor.

The fit to the phases is equally very good (Figures 6b and 6d). In this case there are no vertical strips, only the outliers and again they seem to be absent in the computed values from the model.

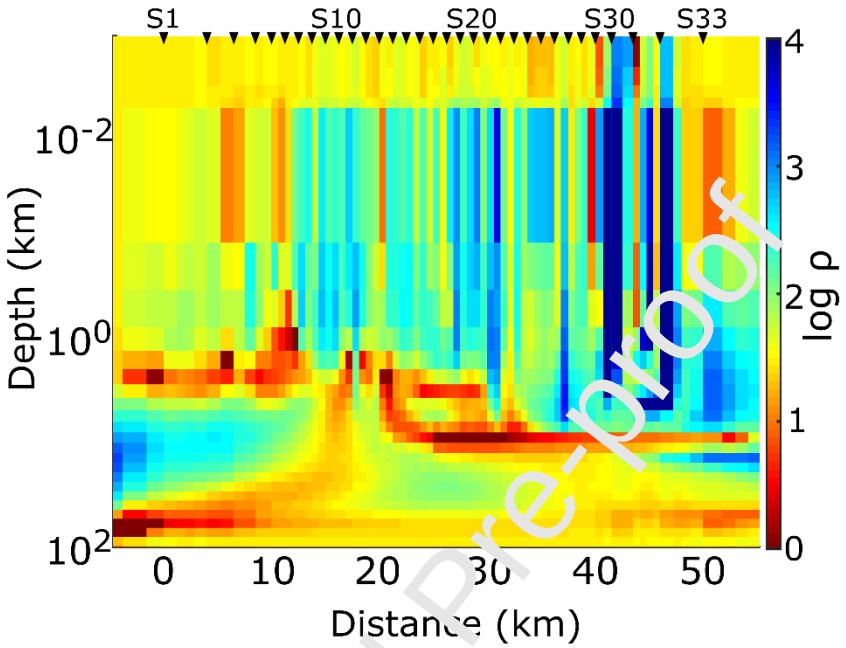

Figure 5. Base model COPROD2S2. The model obtained by inversion of the determinant data shown in Figure 3. The model corresponds to a regularizing factor $\tau = 0.01$.

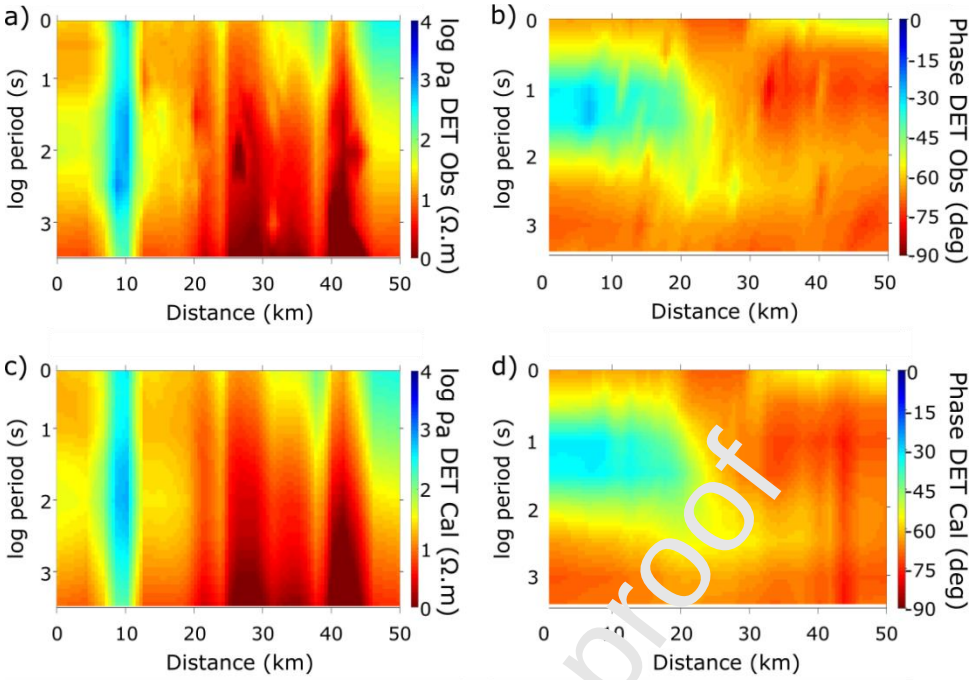

Figure 6. Comparison of the determinant data with the computed values for the base model of the COPROD2S2 dataset. a) and c) show the pseudo-sections of apparent resistivity and b) and d) those of the phases.

As stated earlier, our objective is to get as close as possible to the central all-induction classical sounding. To this end, we compute the TE response of the model of Figure 5. The apparent resistivities and phases are shown in Figure 7. We compare these responses with the original TE data provided by Varentsov (1998). It can be observed in Figures 7a and 7c that the predicted or computed TE apparent resistivities do not show the vertical strips that are present in the original TE data. The colored spots associated with the outliers are also absent in the predicted apparent resistivities. The same applies to the predicted phases. Both the disappearance of the vertical strips and of the local-colored spots speaks well of the robustness of the approach. However, there remains to estimate the predicted model and to compare with other approaches.

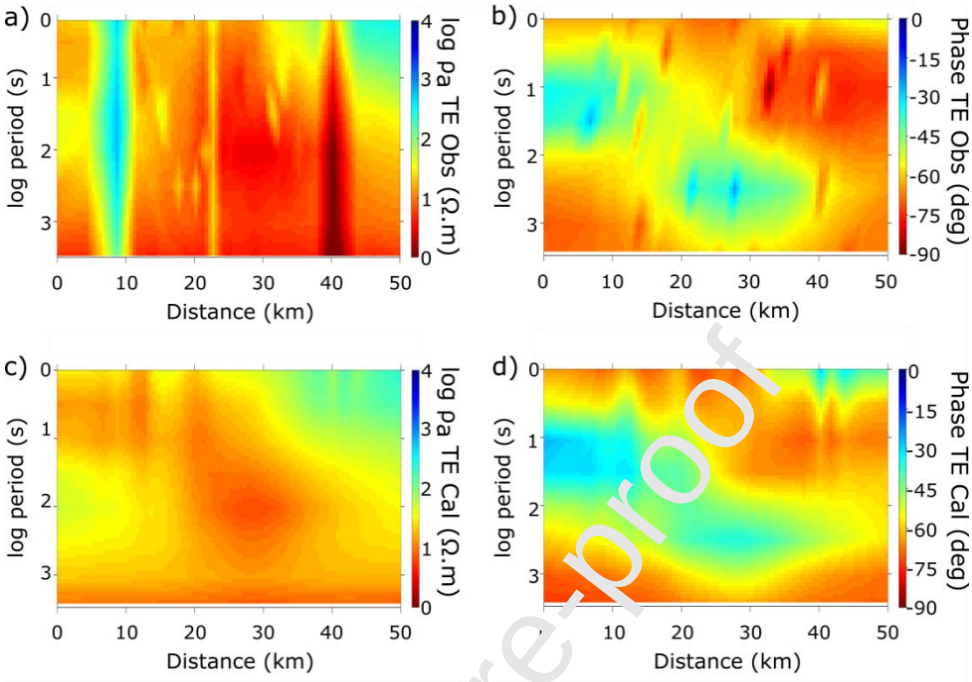

Figure 7.a) The original TE apparent resistivity data and b) the corresponding phase data. c) The computed TE apparent resistivity values and d) the corresponding phase values. The computed TE responses corresponded to the base model shown in Figure 5.

The objective of our approach is to get as close as possible to the classical, central all-induction sounding. If this approach is going to be of any good for routinely interpret MT data the final model must somehow recover the main features of the true model. Figure 8 presents our proposed model for the challenge posed by Varentsov (1998,2002). It is the 1D inversion of the apparent resistivities shown in Figure 6b using the formula for depth averages of electrical conductivity given by Gómez-Treviño (1996). The model is a smooth version of those obtained

by Ogawa (1999) and Gómez-Treviño et al. (2014) using other methods. This is as expected since the present approach is the most central or rotational invariant.

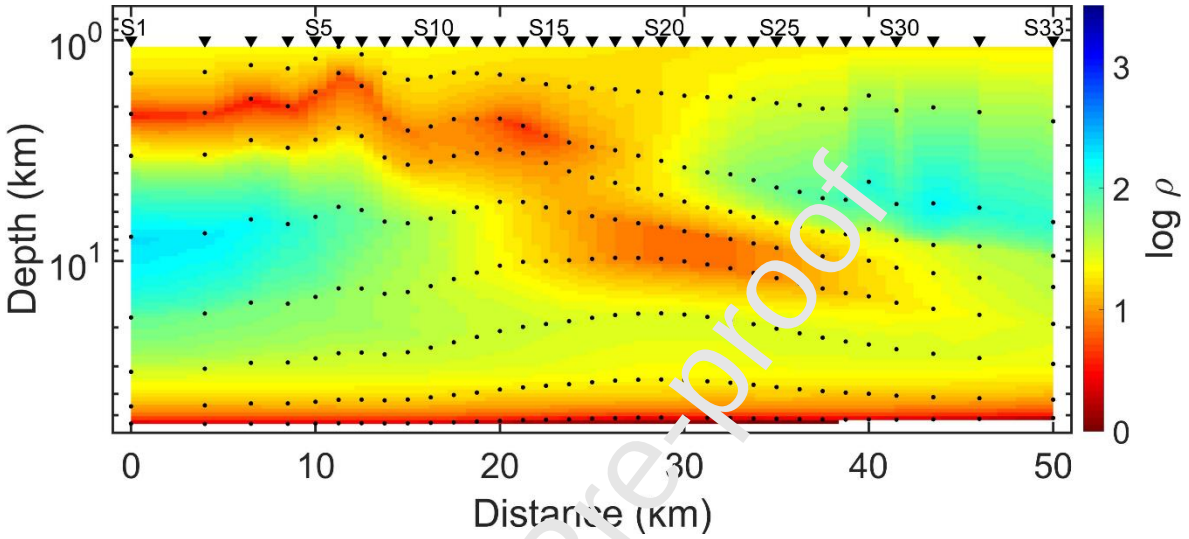

Figure 8. This image represents the view of the classical MT sounding of the COPROD2S2 dataset of Varentsov (1998). The dots represent the depth averages of electrical conductivity.

There is still another way to compare the performance of our approach with the results of other authors. This is by means of the static factors that were used by Varentsov (1998) to distort the data. To estimate these factors, we use

$$\mathrm{sf_{TM}} = \frac{\rho_{\mathrm{aTM}}(\mathrm{data})}{\rho_{\mathrm{aTE}}(\mathrm{model})} \qquad (13)$$

and

$$\mathrm{sf_{TE}} = \frac{\text{Geometric mean } \rho_{\mathrm{aTE}}(\mathrm{data})}{\text{Geometric mean } \rho_{\mathrm{aTE}}(\mathrm{model})} \ . \qquad (14)$$

For the static factor of the TM mode sf_{TM} we use the TM apparent resistivity data of the first period and divide it by the corresponding TE apparent resistivity computed from the model. The assumption is that the two curves begin at the same level for the short periods and that the TE apparent resistivities from the model present no static effects, which they don't. The estimation of the static factors for the TE mode sf_{TE} can also be computed the same way. However, in this case we can use all values of the curves as in equation 14 because the curves are parallel to each other, at least in principle. Our estimates are shown in Figure 9a. The results confirm that the vertical strips of high resistivities on the left-hand side of Figure 2, which are also in the determinant data in Figure 3, are due to static effects. And the same for the vertical strips of low resistivities to the right end of the profile. Figure 9b shows the results reported by Gómez-Treviño et al. (2014) who also obtain a version of an all-induction response using the TM data and the phases of the TE mode. Figure 9c shows the results obtained by Ogawa (1999) who includes the static factors as unknowns in the inverse process, and of Tournerie et al. (2007) who used the cokriging method to estimate the factors without having to obtain a physical model of the subsurface.

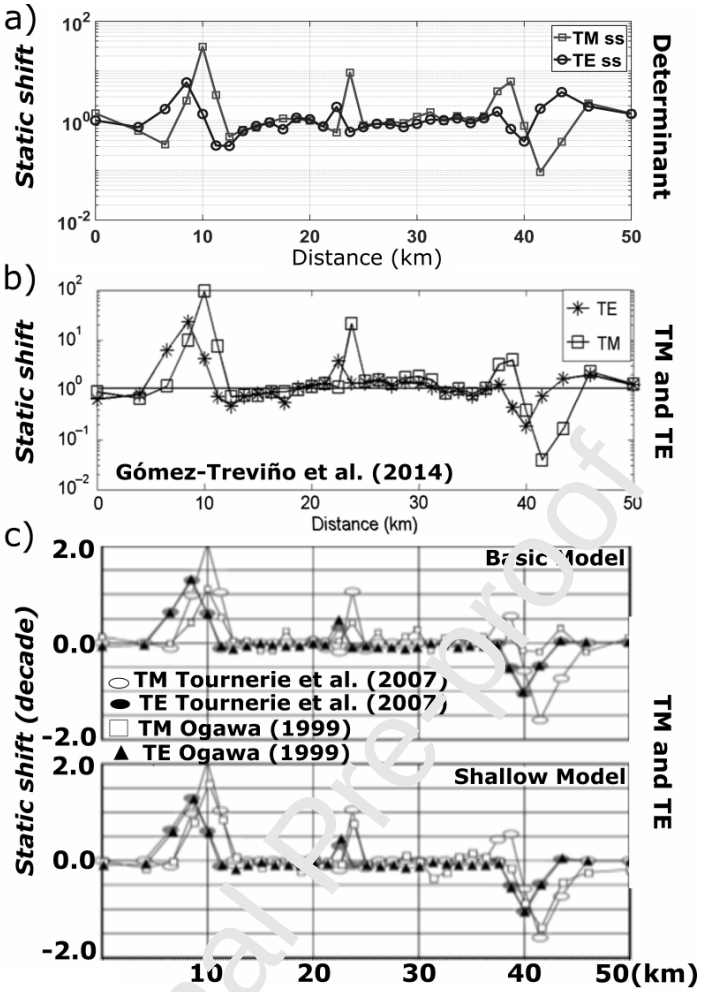

Figure 9. a) The static factors estimated in the present work using determinant data. b) The static factors estimated by Gómez-Treviño et al. (2014) using TE and TM data. c) The static factors as computed and reported by Tournerie et al. (2007) who include the comparison with the results of Ogawa (1999).

3.1 Field data, variable statics and oblique profiles

For the first application to field data, we use 17 MT sites from the BC87 dataset which were recorded in southern British Columbia, Canada. We use the full

tensor of the processed data available at the MTNet website. The length of the profile is about 120 km. The data were recorded for periods ranging from 0.002 to 1800 s and are affected by galvanic distortions (Jones, 1993). As can be seen in Figure 10 the MT profile begins in the Valhalla Complex, crossing the Nelson Batholith, the Kootenay Arc and ends on the Purcell Anticlinorium. Along with the interpretation of the original data we also consider modifications of the static effects and of the directionality of the profile.

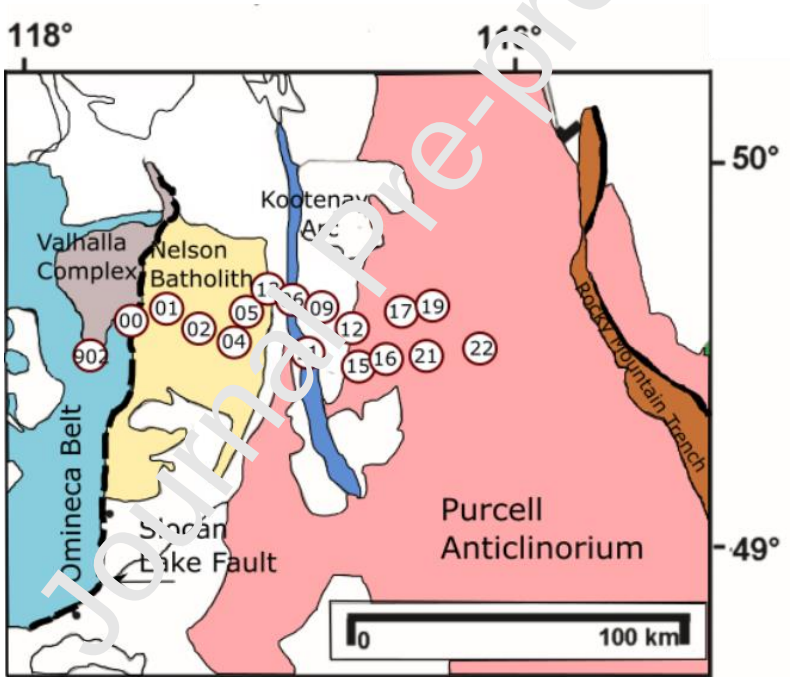

Figure 10. Location of the MT sites selected from the BC87 dataset. The data selected fall on a profile approximately 120 km long east-west.

Figure 11 shows how the geometric averages of the computed TE apparent resistivities converge for $\tau = 0.01$. The corresponding model for this regularization parameter is shown in Figure 12, and the comparison of measured data with the

computed response of the model is shown in Figure 13. It can be observed that most features of the data are reproduced by the response of the model. This means that the model is rough enough and that it recovers as much as possible the small spatial wavelengths. Still, the computed data are smoothed versions of the observed sections, which means that the outliers were not modeled.

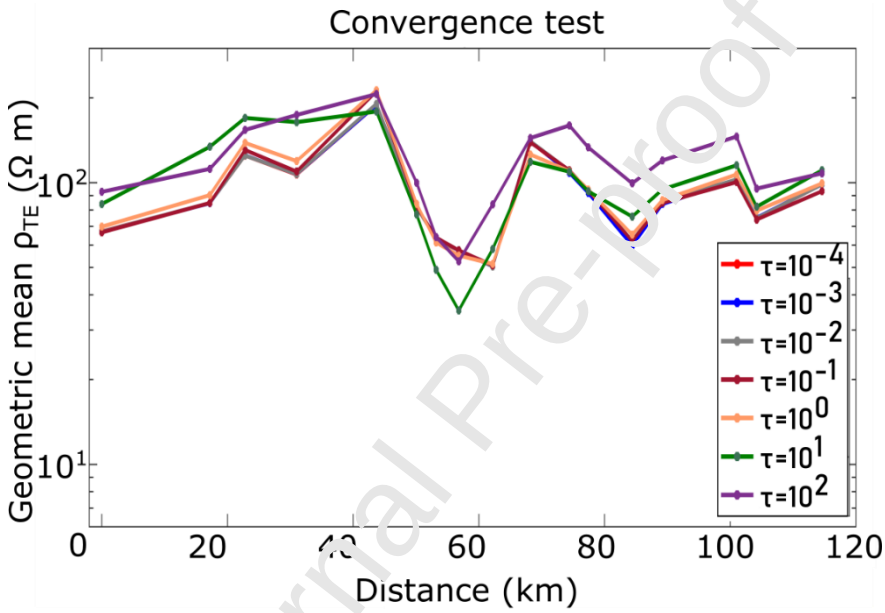

Figure 11. Convergence BC87. Convergence of the geometric mean of the computed TE apparent resistivities for the 17 sites of BC87 dataset. Notice that the curves lower than $\tau = 0.01$ are identical.

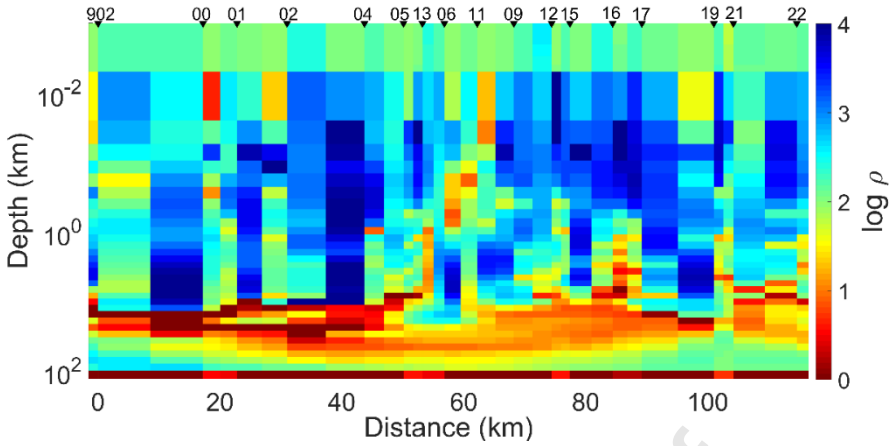

Figure 12. Base model BC87. Model obtained by inversion of the determinant data BC87 data. The model corresponds to the regularizing factor $\tau = 0.01$.

The central all-induction soundings for the different sites are obtained as the TE responses of the rough model shown in Figure 12 for the same sites. The amplitude and phase responses are plotted in Figure 14. To obtain the 2D image we use only the apparent resistivity values because the formula for the depth averages of electrical conductivity does not require the phases. The final image is shown in Figure 15.

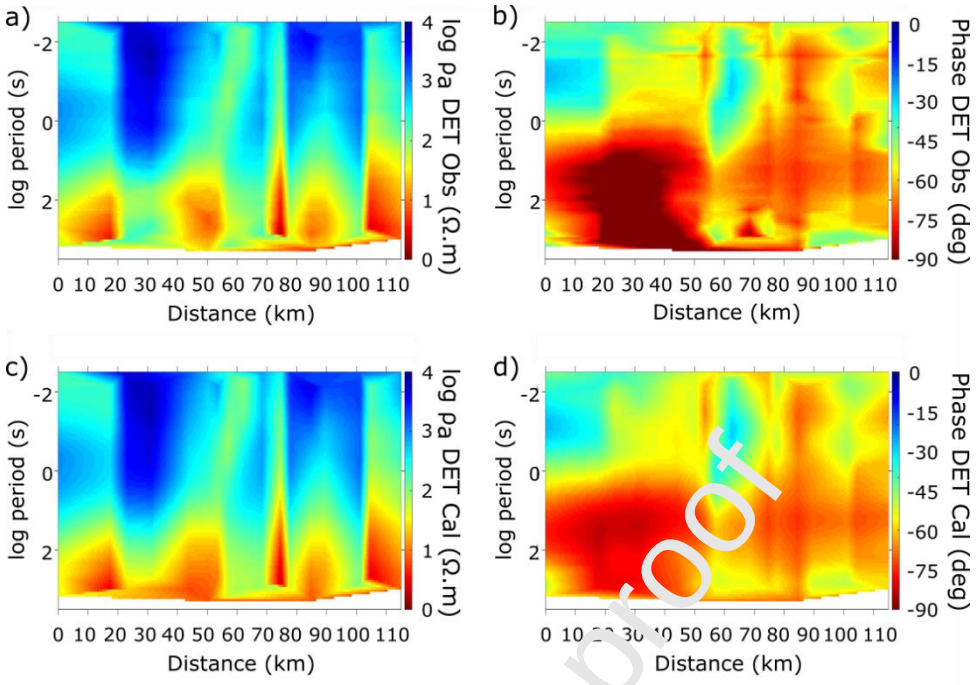

Figure 13. Comparison of determinant observed and computed BC87. a) Magnitude and b) phase of the determinant apparent resistivity obtained from the 17 sites of the BC87 data sets. c) Magnitude and d) phase of the determinant computed from the response of the best model shown in Figure 12.

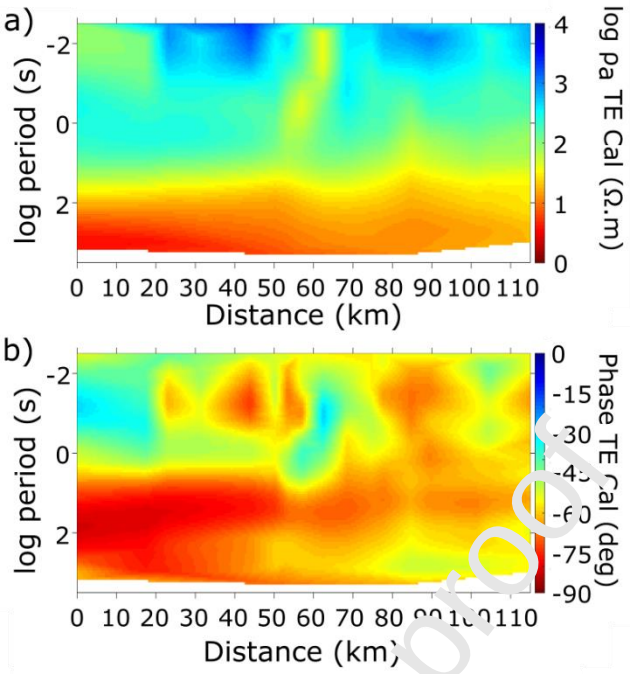

Figure 14. TE responses of the model of Figure 12. a) Apparent resistivities and b) phases.

The 2D image of Figure 15 was obtained by 1D inversion of the apparent resistivities of Figure 14a. Notice how the different geological regions displayed in Figure 10 correlate with the position of the anomalies seen in the image. We place the Slocan Lake Fault (SLF) in our model according to the results reported by Cook et al. (1988); this fault delineates the eastern boundary of the Valhalla complex. Jones et al. (1988) proposed the base of the Nelson Batholith as a transition from highly resistive layer to a less resistive one at a depth of some 5 ±2 km. We also see that change but to a depth of around of 3km. The dominant feature in the model is the deep conductor anomaly which goes through the profile with an approximately depth of 18 km below the Nelson Batholith, to about 5 km below the

Purcell Anticlinorium. This conductor correlates with the North America Cratonic Basement observed in the seismic refraction study of Clowes et al. (1995).

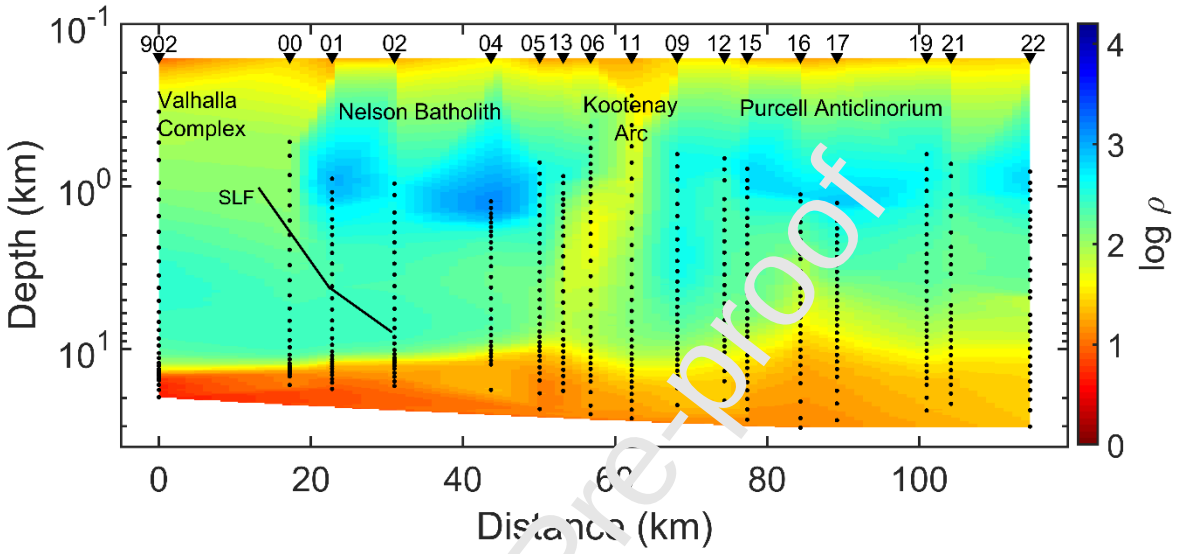

Figure 15. 2D image obtained by 1D inversion of the apparent resistivities of Figure 14a. The dots represent the depth of penetration for the different periods for each site.

Our approach comes particularly handy in cases where there is doubt about the strike direction. In fact, there is always a 90 degrees ambiguity that is usually resolved using independent data, either geological or geophysical. Still, the ambiguity is always present as a real possibility. The BC87 dataset has actually been interpreted assuming the two possibilities because of partial evidence on either side. Jones et al. (1993) assumed a strike N30^{o}W and Eisel and Bahr (1993) used N60^{o}W. Gómez-Treviño et al. (2018) considered both possibilities and were able to predict an EMAP line over the Nelson Batholith assuming a variable strike

centered on N60°W. As stated earlier, our approach avoids having to choose a preferred strike because of the use of the determinant, while it keeps at the same time the desired all-induction property of the classical sounding.

To test the robustness of the approach we experimented with the BC87 data set in two different ways. We modified the apparent resistivities multiplying them by factors to simulate different static effects. Figure 16 shows three scenarios with factors 1, 2 and 3. The computed pseudo-sections of the determinant apparent resistivities are shown in Figures 16a, c and e. It can be observed that as the factors increase the images gradually become darker or show a shift towards the blue, as they should. However, as seen in Figures 16b, d and f the computed TE apparent resistivities for the different factors are practically identical. This means that the roughest model in each case accounts for the different static factors providing the same all-induction responses.

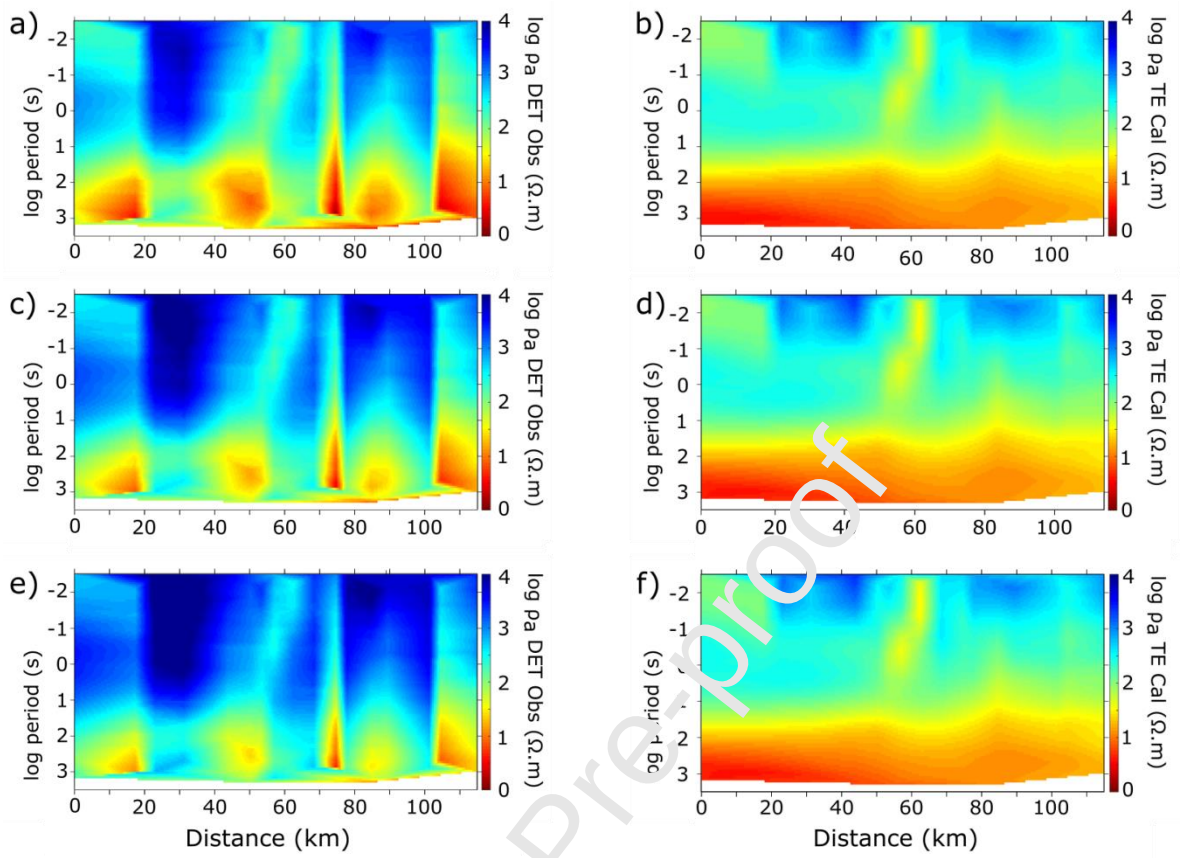

Figure 16. Multiplied apparent resistivities. a, c and e show the determinant apparent resistivities computed from the roughest models that fit the scaled data as multiplied by factors of 1, 2 and 3, respectively. Notice the gradual shift towards the blue. The computed TE apparent resistivities for the different factors are practically identical as shown in b, d and f.

The other experiment we did was to assume different strikes in the interpretation. In the previous application even though we knew that the strike was around N60^{o}W the inversion was affected assuming that the profile was perpendicular to strike. Because we are using an invariant under rotation the data to be inverted is the same regardless of the assumed strike. The only thing that changes is the separation between the sites as shown in Figure 17. Let *a* be a

measure of the original distance between the sites, the new distance between sites thus will be *a/cos(θ)*, where *θ* is the angle of the oblique profile. Regardless of the profile the corresponding sites have exactly the same sounding curves.

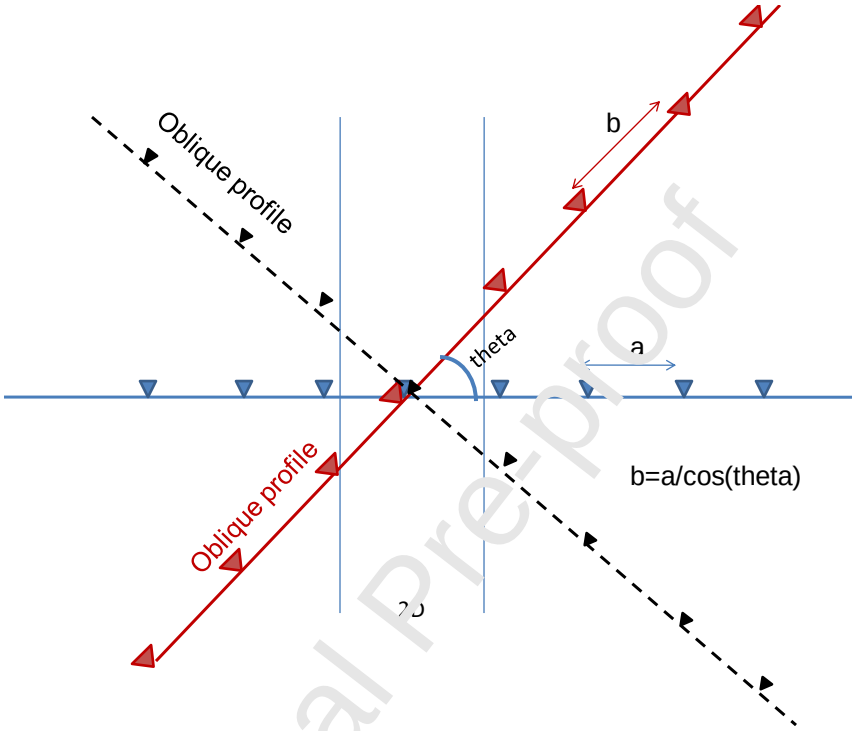

Figure 17. Oblique profiles. The data to be inverted in each profile at the corresponding sites is exactly the same. The only thing that changes is the separation between the sites.

Figure 18 presents the results for the different assumed profiles. Figures 18a, c and e correspond to the data as expanded assuming strikes of 0°, 30° and 45°, respectively. These strikes correspond to expansion factors of the horizontal scale of 1.00, 1.15 and 1.41, respectively. Figures 18b, d and f present the corresponding computed TE responses of the roughest models in the 2D inversions. It can be observed that besides the expected elongation of the profile, the recovered all-induction data are practically identical below the corresponding

sites. This shows that the prediction of the TE data is only weakly dependent on the assumed strike direction. It must be emphasized that we are fitting a 2D model to the determinant data not so much because the data are 2D, but because we are after responses that are free from the effect of electric charges from all depths. The only valid response with this characteristic is the theoretical response of the TE mode of a 2D model. Rather than projecting over the estimated strike we prefer to keep the original separations and positions because what we are after is an all-induction response for the field site, and as discussed above these responses do not change very much when rotating the profile.

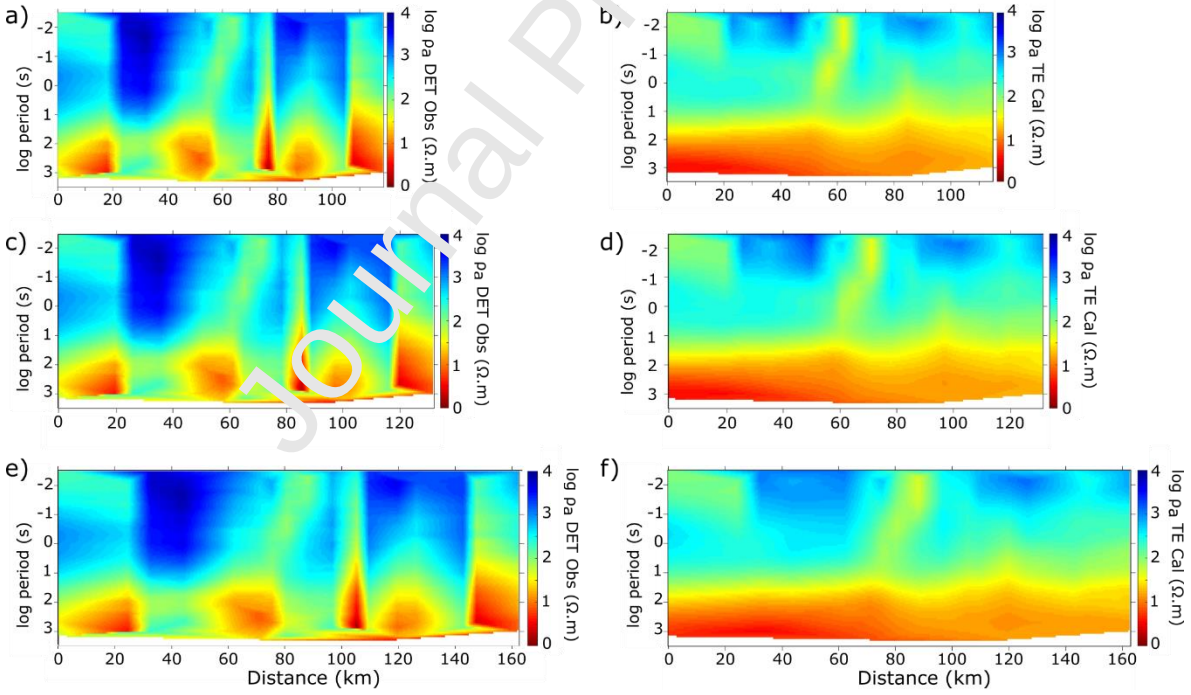

Figure 18. Figures 18a, c and e correspond to the data as expanded assuming strikes of 0°, 30° and 45°. These strikes correspond to expansion factors of the horizontal scale of 1.00, 1.15

and 1.41, respectively. Figures 18b, d and f present the computed TE responses of the roughest models in the 2D inversions.

3.2 Guzman field data and the detection of a magma reservoir

The second application to field data corresponds to a profile localized in the western sector of the Trans-Mexican Volcanic Belt (TMVB), specifically in the central region of the Colima Graben (Figure 19). The GUZMAN profile (GUZ) has 9 MT sites (G1 to G9) with an overall length of 120 km (Guevara-Betancourt; 2017; 2020). The line crosses perpendicular the Colima Volcanic Complex (CVC) composed of three volcanoes: El Cántaro (EC), Nevado de Colima (NC) and Volcán de Colima (VC). This last is an active volcano. The data were registered with 3 channels for the magnetic field (Hx, Hy and Hz) and 2 channels for the electric field (Ex, Ey) with a period range from 0.01 to 1000 s. The zone has rugged topography, large composite volcanoes and complex normal fault structures with N-S and NNE-SSW orientations (Allan, 1986) that could produce distortions on the electric field.

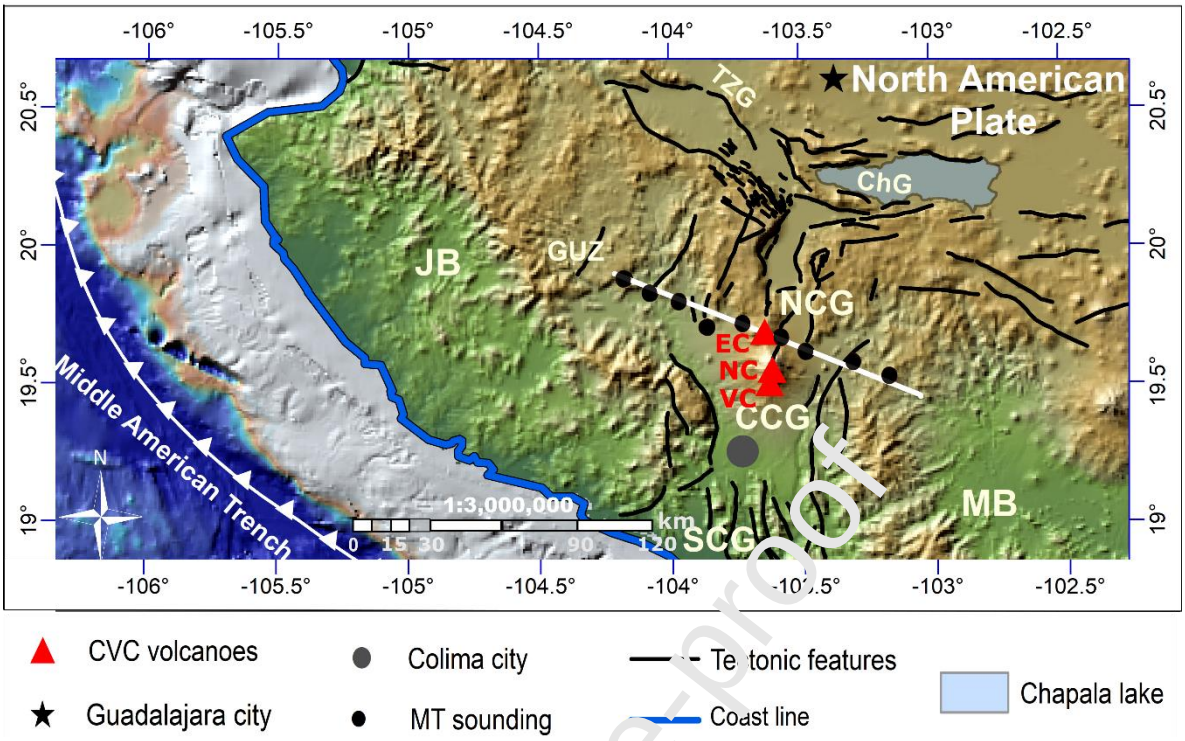

Figure 19. Location of GUZMAN profile. Distribution of the 9 MT sites. The GUZ survey is between the Central Colima Graben (CCG) and the North Colima Graben (NCG), to the south of the Tepic-Zacoalco Graben (TZG) and Chapala Graben (ChG). The profile crosses the Colima Volcanic Complex, near the El Cántaro (EC) and El Nevado de Colima (NC) volcanoes, further south is Volcán de Colima (VC) volcano. The figure also shows the subduction of the Cocos and Rivera plates beneath the Middle America Trench. The GUZMAN line is over a fraction of the Jalisco Block (JB) and Michoacan Block (MB).

Like in the previous cases, we first make the convergence test by lowering the smoothing parameter as much as possible in the 2D algorithm. The convergence graph is shown in Figure 20. It can be observed that the geometric averages of the TE apparent resistivities converge for values equal or smaller than the parameter $\tau = 0.1$. We use this value to obtain the model shown in Figure 21. It is worth remarking that this is the roughest possible model that fits the data. As explained earlier, the idea is to recover as many details as possible but keeping on the safe side. Using the largest of the regularizing parameters at convergence prevents unrealistic values of electrical resistivity that may distort the final model.

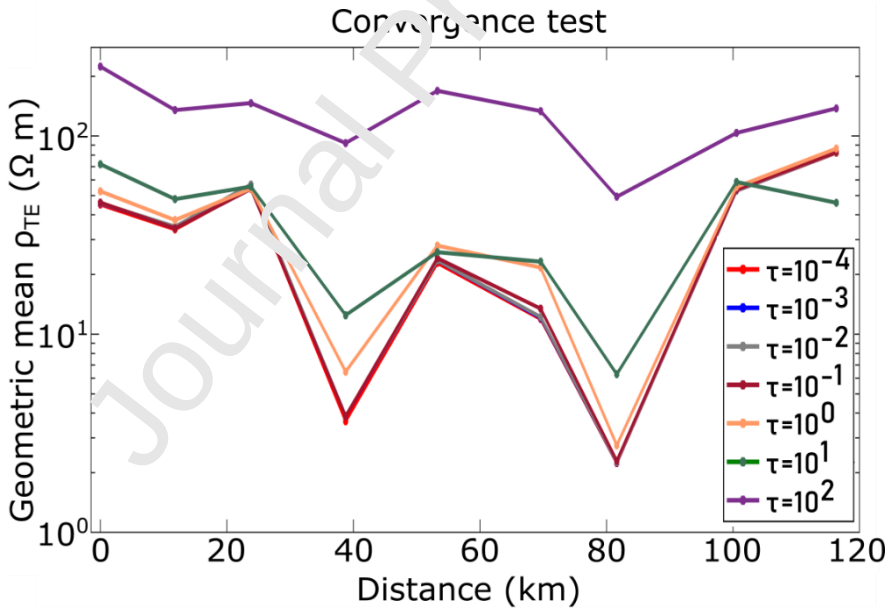

Figure 20. Convergence GUZMAN. Convergence of the geometric mean of the TE computed apparent resistivities for the 9 sites of GUZ line. Notice that the curves from $\tau = 0.1$ are identical. The curves converge for < 0.01 .

The observed and the computed determinant data are displayed in Figure 22. It can be observed that the responses of the model reproduce the main features of the data, except for the high frequency noise that shows as alternate thin horizontal strips. The clean data is computed as the TE responses of the roughest model and are shown in Figure 23 for both apparent resistivities and phases. For the final all-induction model, we use only the apparent resistivities as before. The final model for the GUZMAN profile is shown in Figure 24.

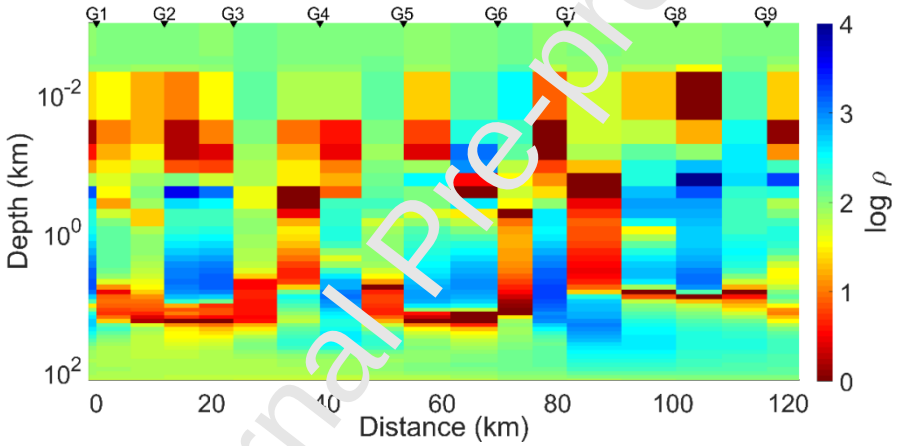

Figure 21. Base model GUZMAN. Model obtained by inversion suing the regularization para meter $\tau = 0.1$ of the determinant data of GUZ line.

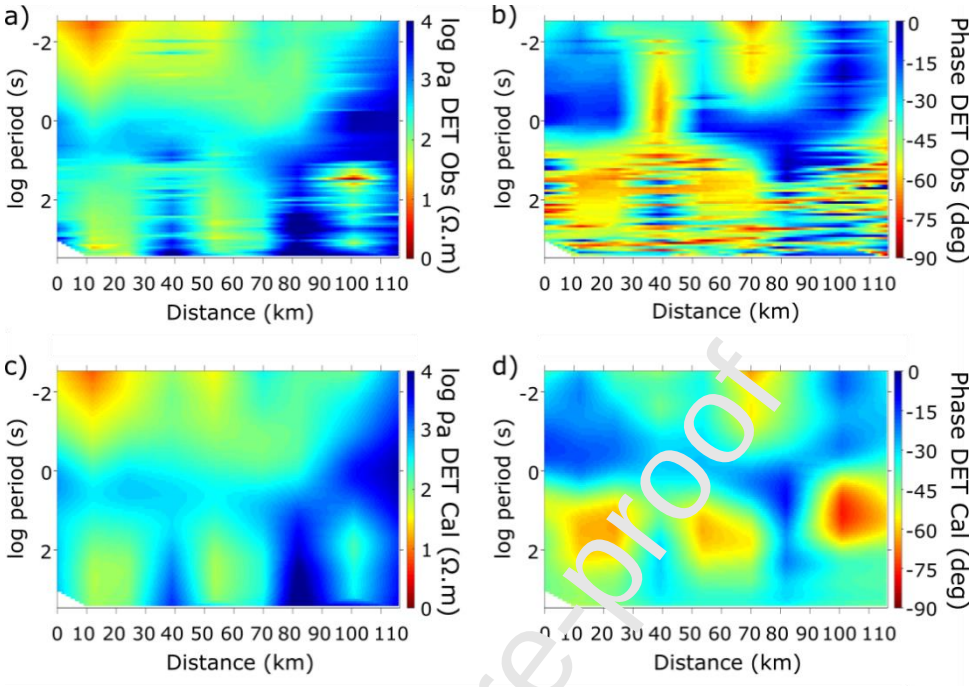

Figure 22. Comparison of determinant observed and computed in GUZMAN profile. a) Magnitude and b) Phase of the determinant apparent resistivity obtained for the GUZ line. c) Magnitude and d) Phase determinant computed from the response of the model shown in Figure 21.

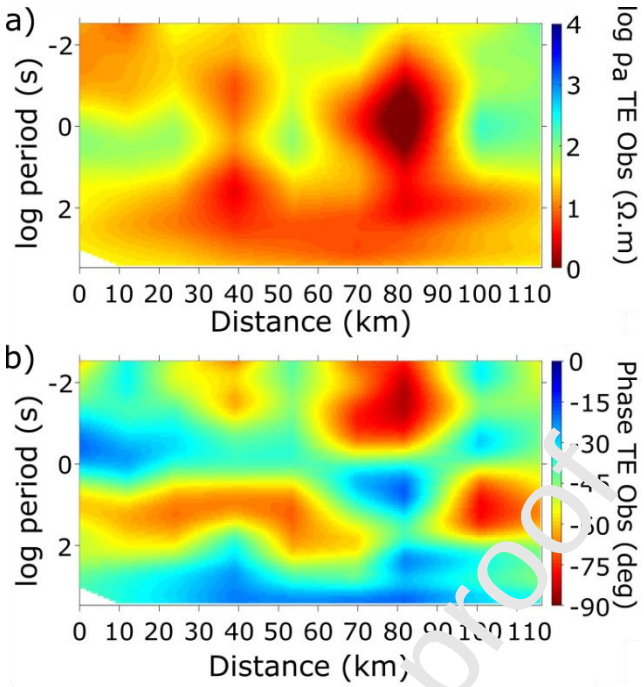

Figure 23. a) and b) show the computed TE apparent resistivities and phases, respectively, computed for the model shown in Figure 21.

It can be observed in Figure 24 that there are two localized shallow conductors, one below site G4 and the other below sites G6 and G7. These can be associated to local faults according to the map in Figure 19. There is also a somewhat continuous deep conductor from a depth of about 10 to 30 km that tends to be shallower and thinner to the east below sites G7, G8 and G9. This can be associated to the existence of a magma reservoir below the Colima Volcanic Complex. Sychev, et al. (2019) proposed the existence of this reservoir on the basis of seismic tomography in relation with the active VC volcano. Although the GUZMAN profile crosses the Colima Graben about 10 km north of the active volcano, it still senses the existence of this reservoir. There is evidence that the volcanic activity has been migrating to the south towards the present active VC

volcano (e.g., Alvarez and Yutsis, 2015; Sychev, et al., 2019), tough Romo-Lozano and Arzate-Flores (2020) indicates that there is no shallow magma chamber south the CVC. Our results would imply that the magma reservoir is still present in the northern part of the Colima Graben.

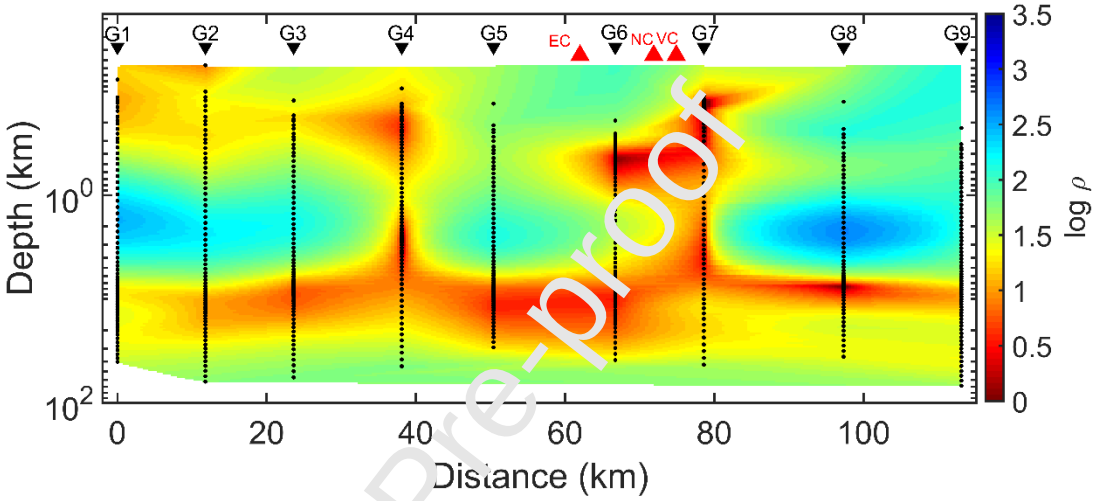

Figure 24. All-induction model for GUZMAN dataset. El Cántaro (EC), El Nevado de Colima (NC) and Volcán de Colima (VC) volcanoes are projected to the profile. The dots correspond to the depth of penetration of the estimated averages of electrical conductivity.

It is worth remarking that the type of smoothness attained by removing the effects of electric charges from all depths cannot be achieved applying standard regularization. Consider the model shown in Figure 25 which was obtained using the same algorithm of Rodi and Mackie (2001) as for the roughest model of Figure 21. In this case we applied the criterion of the well-known L-curve (Hansen,1998) to determine the balance between the roughness of the model and the fit to the data. The model bears some resemblance to the roughest model of Figure 21 but it is somewhat smoother because of the higher penalization on roughness. It also has a better lateral continuity due to a higher density of horizontal cells. The model also resembles the all-induction image of Figure 24 except for the many shallow conductors and deep resistors below the different sites. These anomalies may or may not be real, the point to remark is that those that remain are due solely to electromagnetic induction as in the classical magnetotelluric sounding.

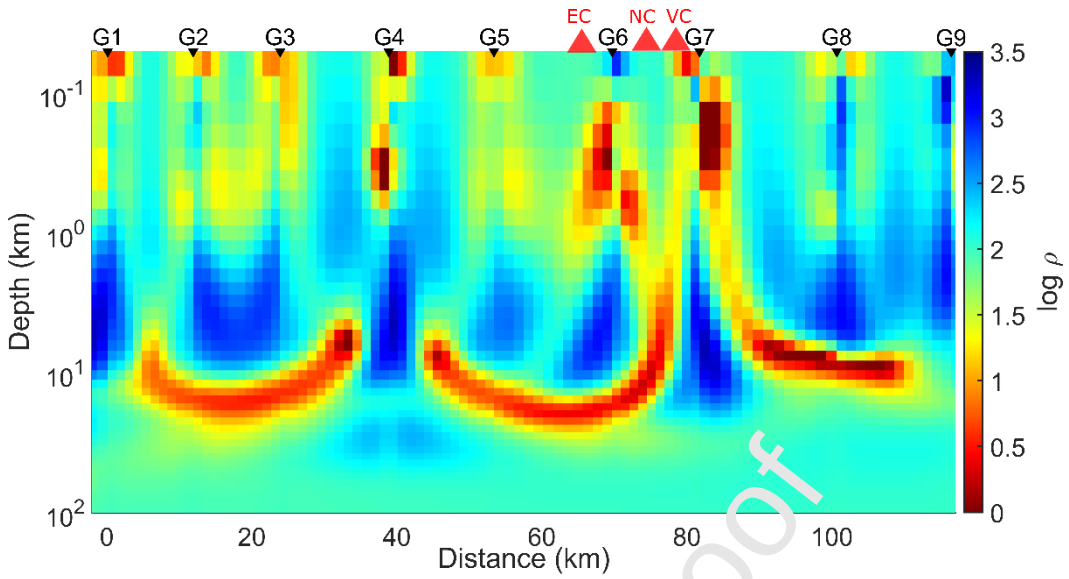

Figure 25. Model for Guzman dataset applying standard regularization. The balance between the roughness of the model and the fit to the data was determined using the criterion of the L-curve. Notice that the localized shallow conductors and deep resistors are not present in the all-induction model of Figure 24.

4. Conclusions

Inverting invariants of the magnetotelluric impedance tensor is not new. Neither are the attempts to isolate electromagnetic induction from responses that contain effects from electric charges at all depths. What is new is the combination that brings us closer to the ideal or classical MT sounding. In fact, we think this is the closest approximation possible. For one thing, no other invariant but the determinant can accommodate in a single factor all the four galvanic distortions. In 2D inversions this factor can be physically modeled and taken care of by the apparent resistivities of the TM mode. Furthermore, a 2D model is the only one that

can provide responses that are free from the effect of electric charges from all depths. It is difficult to imagine another combination that could do better than these two. However, it must be said that in the process there is a loss of lateral resolution because of the elimination of the effect of all electric charges, not only those associated with galvanic distortions. It is a kind of physical regularization that erases all effects except those due to electromagnetic induction. Aside from the purely academic curiosity of how a survey would have looked if it could have been realized with classic MT sounding, there is the practical side of returning to the MT method the particular feature of being a detector of good conductors without the interference of good resistors.

5. Data availability

The COPROD2S2 (Varentsov, 1998) and the BC87 (Jones, 1993) dataset are available on MTNet webpage www.mtnet.info/data/download_data.html. The GUZMAN profile is a private data set from CONACYT 221487 and PAPIIT IN-116816 projects.

6. Acknowledgements

The authors thanks to Consejo Nacional de Ciencia y Tecnología for the postdoctoral scholarship to CVU 292913. The authors are grateful to CONACYT 221487 and PAPIIT IN-116816 projects for financial support in obtaining GUZMAN Field dataset. We recognize material help from J. Arzate. The authors acknowledge LITHOPROBE (Doug Oldenburg, UBC) and the GSC (Alan Jones) for making the BC87 dataset available. We also thank F.J. Esparza for fruitful discussions on the use of the 2D code. The

authors also appreciated the comments of the anonymous reviewers and of editor Mark Everett.

7. References

Allan, J.F., 1986. Geology of the Northern Colima and Zacoalco grabens, southwest Mexico: Late Cenozoic rifting in the Mexican Volcanic Belt. Geol. Soc. Am. Bull. 97, 473–485. https://doi.org/10.1130/0016-7606(1986)97<473:GOTNCA>2.0.CO;2.

Alvarez, R., Yutsis, V., 2015. Southward migration of magmatic activity in the Colima Volcanic complex, Mexico: An ongoing process. International Journal of Geosciences, 06 (09), 1077–1099. https://doi.org/10.4236/ijg.2015.69085.

Bahr, K., 1988. Interpretation of the magnetotelluric impedance tensor, regional induction and local telluric distortion. J. Geophys., 62(1),119-127.

Berdichevsky, M.N., Dmitriev, V.I., 1976. Basic principles of interpretation of magnetotelluric curves. In: Geoelectric and Geothermal Studies, (ed) Adam, A., Akademini Kiado. pp. 165–22.

Berdichevsky, M.N., Dmitriev, V.I., Pozdnjakova, E.E., 1998. On two-dimensional interpretation of magnetotelluric soundings. Geophys. J. Int. 133, 585–606. https://doi.org/10.1046/j.1365-246X.1998.01333.x.

Bostick, F.X., 1977. A simple almost exact method of magnetotelluric analysis. In: Ward, S., Ed., Workshop of Electrical Methods in Geothermal Exploration, Univ. of Utah Res. Inst., U. S. Geol. Surv. Contract 14-08- 0001-g-359.

Bostick, F.X., 1984. Electromagnetic array profiling survey method: U.S. patent 4,591,79.

Bostick, F.X., 1986. Electromagnetic Array Profiling (Expanded Abstract) Soc. Expl. Geophys. 56th Ann. Mtg. Houston Tx.

Cagniard, L., 1953. Basic theory of the magneto-telluric method of geophysical prospecting. Geophysics.18, 605–635.https://doi.org/10.1190/1.1437915.

Clowes, R.M., Zelt, C.A., Amor, J.R., Ellis, R.M., 1995. Lithospheric structure in the southern Canadian Cordillera from a network of seismic refraction lines. Can. J. Earth Sci. 32,1485–1516.https://doi.org/10.1139/e95-122.

Constable, S.C., Parker, R.L., Constable, C.G., 1987. Occam's inversion: a practical algorithm for generating smooth models from electromagnetic sounding data. Geophysics. 52, 289–300.https://doi.org/10.1190/1.1442303.

Cook, F.A., Green, A.G., Simony, P.S., Price, R.A., Parrish, R.R., Milkereit, B., Gordy, P.L., Brown, R.L., Coflin, K.C., Patenaude, C., 1988. LITHOPROBE seismic reflection structure of the southeastern Canadian Cordillera: initial results. Tectonics. 7, 157-180. https://doi.org/10.1029/TC007i002p00157.

Eisel, M., Bahr, K., 1993. Electrical anisotropy in the lower crust of British Columbia: an interpretation of a magnetotelluric profile after tensor decomposition. Journal of Geomagnetism and Geoelectricity. 45, 1115–1126, https://doi.org/10.5636/jgg.45.1115.

Esparza-Hernández, F.J., Gómez-Treviño, E., 1997. Implications of spatial filtering on the resolving power of magnetotelluric data. Phys. Earth Planet. Inter. 99, 113–119. https://doi.org/10.1016/S0031-9201(96)03181-0.

Feucht, D.W., Sheehan, A.F., Bedrosian, P.A., 2017. Magnetotelluric Imaging of Lower Crustal Melt and Lithospheric Hydration in the Rocky Mountain Front Transition Zone, Colorado, USA. J. Geophys. Res. Solid Earth. 122, 9489-9510. https://doi.org/10.1002/2017JB014474.

Gómez-Treviño, E., 1996. Approximate depth averages of electrical conductivity from surface magnetotelluric measurements. Geophys. J. Int.127, 762–772. https://doi.org/10.1111/j.1365-246X.1996.tb04055.x.

Gómez-Treviño, E., Esparza, F.J., Romo Jones, J.M., 2013. Effect of galvanic distortions on the series and parallel magnetotelluric impedances and comparison with other responses. Geofis. Int. 52,135–152.

Gómez-Treviño, E., Esparza, F., Muñiz, Y., Calderón, A., 2014. The magnetotelluric transverse electric mode as a natural filter for static effects: application to the COPROD2 and COPROD2S2 data sets. Geophysics. 79, E91–E99. https://doi.org/ 10.1190/geo2012-0522.1.

Gómez-Treviño, E., Muñiz, Y., Cuellar, M., Calderón-Moctezuma, A., 2018. Invariant TE and TM magnetotelluric impedances: application to the BC87 dataset. Earth Planets Space. 70, 133. https://doi.org/10.1186/s40623-018-0900-y.

Groom, R., Bailey, R.C., 1989. Decomposition of magnetotelluric impedance tensors in the presence of local three-dimensional galvanic distortions. J. Geophys. Res. 93, 1913-1925. https://doi.org/10.1029/JB094iB02p0191.

Guevara-Betancourt, R., Arzate, J.A., Yutsis, V., Almaguer, J., 2017. Discontinuidad cortical continental entre las placas de Rivera y Cocos y el sistema de cámaras magmáticas del complejo volcánico de Colima mediante sondeos magnetotelúricos y gravimetría satelital. Congreso Internacional de la RAUGM, Puerto Vallarta, Mex., Oct., 2017. Geos 37(1),30.

Guevara-Betancourt, R.E., 2021. Determinación del límite entre los Bloques de Jalisco y Michoacán a lo largo del Graben de Colima y su influencia sobre el Complejo Volcánico de Colima mediante Métodos Geofísicos. PhD Thesis. Instituto Potosino de Investigación Científica y Tecnológica (IPICYT), San Luis Potosí, México, 152 pp.

Hansen, P.C., 1998. Rank-deficient and discrete ill-posed problems: numerical aspects of linear inversión. Society for Industrial and Applied Mathematics, Philadelphia. https://doi.org/10.1137/1.9780898719697.

Jiracek, G.R., 1990. Near Surface and Topographic Distortion in Electromagnetic Induction. Surv. Geophys. 11,163-203. https://doi.org/10.1007/BF01901659.

Jones, A.G., Kurtz, R.D., Oldenburg, D.W., Boerner, D.E., Ellis, R., 1988. Magnetotelluric observations along the lithoprobe southeastern Canadian cordilleran transect. Geophys. Res. Lett. 15, 677–680. https://doi.org/10.1029/GL015i007p00677.

Jones, A.G., 1993. The BC87 dataset: tectonic setting, previous EM results, and recorded MT data. Journal of Geomagnetism and Geoelectricity. 45, 1089–1105. https://doi.org/10.5636/jgg.45.1089.

Jones, A.G., Groom, R.W., Kurtz, R.D., 1993. Decomposition and modeling of the BC87 dataset. Journal of Geomagnetism and Geoelectricity. 45,1127–1150. https://doi.org/10.5636/jgg.45.1127.

Mackie, R.L., Madden, T.R., Wannamaker, P.E., 1993. Three-dimensional magnetotelluric modeling using difference equations—Theory and comparisons to integral equation solutions. Geophysics. 58, 215-226.

Montiel-Álvarez, A., Romo-Jones, J.M., Constable, S., Gómez-Treviño, E., 2020. Invariant TE and TM impedances in the marine magnetotelluric method. Geophys. J. Int. 221, 163-177. https://doi.org/10.1093/gji/ggz571.

Muñíz, Y., Gómez-Treviño, E., Esparza, F.J., Cuellar, M., 2017. Stable 2D magnetotelluric strikes and impedances via the phase tensor and the quadratic equation. Geophysics. 82, E169–E186. http://doi.org/10.1190/GEO2015-0700.1.

Ogawa, Y., 1999. Constrained inversion of COPROD-2S2 dataset using model roughness and static shift. Earth Planets Space. 51, 1145-1151. https://doi.org 10.1186/BF03351588.

Pedersen, L., Engels M., 2005. Routine 2D inversion of magnetotelluric data using the determinant of the impedance tensor. Geophysics. 70, G33-G41. https://doi.org/10.1190/1.1897032.

Rikitake, T., 1950. Electromagnetic induction within the Earth and its relation to the electrical state of the Earth's interior. Bull. Earth. Res. Inst. Tokyo Univ. 28, 45-100.

Robertson, R.C., 1989. Interpretation of synthetic three-dimensional magnetotelluric data. J. Geophys. Res. 94B, 4225–4230. https://doi.org/10.1029/JB094iB04p04225.

Rodi, W., Mackie, R.L., 2001. Nonlinear conjugate gradients algorithm for 2-D magnetotelluric inversion. Geophysics. 66, 174-187. https://doi.org/10.1190/1.1444893.

Romo-Jones, J., Gomez-Trevino, E., Esparza, F., 2005. Series and parallel transformations of the magnetotelluric impedance tensor: Theory and applications. Phys. Earth Planet Inter. 150 63-83. https://doi.org/10.1016/j.pepi.2004.08.021

Romo-Jones, J.M., Gomez-Trevino, E., Flores, C., García-Abdeslem, J., 2017. Electrical conductivity of the crust in central Baja California, México, based on magnetotelluric observations. J. S. Am. Earth Sci. 80, 18-28. https://doi.org/10.1016/j.jsames.2017.08.024.

Romo-Lozano, H.M. Arzate-Flores, J.A., 2020. Resistivity model for the Colima Volcanic Complex from magnetotelluric observations, EGU General Assembly 2020, Online, 4-8 May 2020, EGU2020-6188. https://doi.org/10.5194/egusphere-egu2020-6188.

Ruiz-Aguilar, D., Tezkan, B., Arango-Galván, C., Romo-Jones, J.M., 2020. 3D inversion of MT data from northern Mexico for geothermal exploration using TEM data as constraints. J. Appl. Geophy. *172,* 103914.

Rung-Arunwan, T., Siripunvaraporn, W., Utada, H., 2016. On the Berdichevsky average. Phys. Earth and Planet. Inter. *253,* 1-4.

Rung-Arunwan, T., Siripunvaraporn, W., Utada, H., 2017. Use of ssq rotational invariant of magnetotelluric impedances for estimating informative properties for galvanic distortion. Earth, Planets Space. 69, 1-24.

Shi, Y., Xu, Y., Yang, B., Peng, Z., Liu, S., 2020. Three-dimensional audio-frequency magnetotelluric imaging of Zhuxi copper-tungsten polymetallic deposits, South China. J. Appl. Geophy. 172, 103910.

Siripunvaraporn, W., Egbert, G., Lenbury, Y., Uyeshima, M., 2005. Three-dimensional magnetotelluric inversion: data-space method. Phys. Earth Planet. Inter. 150, 3-14.

Sternberg, B., Washburne, J., Pellerin, L., 1988. Correction for static shift in magnetotellurics using transient electromagnetic soundings. Geophysics. 53, 1459-1468.https://doi.org/10.1190/1.1442426.

Sychev, I.V., Koulakov, I., Egorushkin, I., Zhuravlev, S., West, M., El khrepy, S., Al-Arifi, N., Alajmi, M.S., 2019. Fault-Associated Magma Conduits Beneath Volcán de Colima Revealed by Seismic Velocity and Attenuation Tomography Studies. J. Geophys. Res. Solid Earth. 124, 8908-8923.https://doi.org/10.1029/2019JB017449.

Szarka, L., Menvielle, M., 1997. Analysis of rotational invariants of the magnetotelluric impedance tensor. Geophys. J. Int. 129, 133-142. https://doi.org/10.1111/j.1365-246X.1997.tb00942.x

Tikhonov, A.N., 1950. On determining electrical characteristics of the deep layers of the Earth's crust. Doklady Akademii Nauk, SSSR. 73, 295-297.

Torres-Verdín, C., 1991. Continuous profiling of magnetotelluric fields: Ph.D. thesis, University of California, Berkeley.

Torres-Verdín, C., Bostick, F., 1992a. Implications of the Born approximation for the magnetotelluric problem in three dimensional environments. Geophysics. 57, 587–602.https://doi.org/10.1190/1.1443272.

Torres-Verdín, C., Bostick, F.X., 1992b. Principles of spatial surface electric field filtering in magnetotellurics: Electromagnetic array profiling (EMAP). Geophysics. 57, 603–622.https://doi.org/10.1190/1.1443273.

Tournerie, B., Chouteau, M., Marcotte, D., 2007. Magnetotelluric static shift: Estimation and removal using the cokriging method. Geophysics. 72,12JF-Z15. https://doi.org/10.1190/1.2400625.

Varentsov, I.M., 1998. 2D synthetic data sets COPROD-2S to study MT inversion techniques: Presented at the 14th Workshop on Electromagnetic Induction in the Earth. Data available at https://www.mtnet.info/main/ website.

Varentsov, I.M., 2002. A general approach to the magnetotelluric data inversion in a piecewise continuous media. Phys. Solid Earth. 38, 913–934.

Wang, K., Cao, H., Duan, C., Huang, J., Li, F., 2019. Three-dimensional scalar controlled-source audio-frequency magnetotelluric inversion using tipper data. J. Appl. Geophys. 164, 75-86.

Wang, S., Constable, S., Reyes, V., Jahandaril H., Farquharson, C., Avilés-Esquivel, T., 2020. Two-dimensional determinant inversion of marine

magnetotelluric data and a field example from the Gulf of California, Mexico. Geophysics. 86, 1-63. https://doi.org/10.1190/geo2019-0735.1.

Zhdanov, M.S., Keller, G.V., 1994 The Geoelectrical Methods in Geophysical Exploration, Elsevier Science.

Declarations

"How close can we get to the classical magnetotelluric sounding?"

By A. Calderón-Moctezuma, E. Gomez-Treviño, V. Yutsis and R. Guevara-Betancourt, Marianggy Gómez-Ávila

Funding: Armando Calderon-Moctezuma was funded by a Posdoctoral scholarship from *"Estancias Posdoctorales Vinculadas al Fortalecimiento de Calidad del Posgrado Nacional, 2018(1)", CONACYT*. CVU: 292913.

Conflicts of interest/Competing interests: The authors declare no conflict of interest.

Code availability: Not applicable.

CREdiT or Authors' contributions:

A. Calderón-Moctezuma: Conceptualization, Investigation, Software, Visualization, Formal analysis, Writing-Original draft preparation.

E. Gomez-Treviño: Conceptualization, Investigation, Writin-Original draft preparation, Writing-Review & Editing.

V. Yutsis: Supervision, Project administration and Review, Funding acquisition.

R. Guevara-Betancourt: Data Curation, Validation, Writing-Review & Editing.

Marianggy Gómez-Ávila: Formal Analysis, Visualization, Geological review, Writing-Review & Editing.

Declaration of interests

☒ The authors declare that they have no known competing financial interests or personal relationships that could have appeared to influence the work reported in this paper.

☐The authors declare the following financial interests/personal relationships which may be considered as potential competing interests:

Highlights

- Resistivity image free from galvanic distortions.
- Splitting of rotational invariant data into orthogonal TE and TM modes.
- Using of the TE mode as natural filter for the effect of electric charges.
- Detection of magma reservoir below the Colima Volcanic Complex.